Dalton Transactions

ROYAL SOCIETY OF CHEMISTRY

PAPER

View Article Online
View Journal | View Issue

Cite this: *Dalton Trans.*, 2024, **53**, 13982

Reductive hydrothermal conversion of uranyl oxalates into UO_{2+x} monitored by *in situ* XANES analyses†

Sofian Benarib, [a] Maëva Munoz, [a] Isabelle Kieffer, [b] Jean-Louis Hazemann, [c] Nicolas Dacheux [a] and Nicolas Clavier *[a]

Hydrothermal conversion of actinide oxalates has recently gained attention as an innovative fabrication route for nuclear fuels but has remained mainly limited to tetra- or tri-valent cations. We report herein the reductive conversion of mixtures of uranyl and oxalate ions into UO_{2+x} oxides under mild hydrothermal conditions (T = 250 °C). A multi-parametric study first led to specifying the optimal conditions in terms of pH, oxalate/U ratio and duration to provide a quantitative precipitation of uranium in the hyperstoichiometric dioxide form with pH = 0.8; $R = n_{oxalate}/n_U = 3$, and t = 72 hours. Particularly, pH was evidenced as a key parameter, with 3 different compounds obtained over a range of only 0.4 units. The mechanism leading to the formation of UO_{2+x} was then investigated thanks to an *in situ* XANES study. Analysis of the supernatant showed that U(VI) was quickly reduced into U(IV) thanks to the presence of oxalates and/or their decomposition products in solution, following first-order kinetics. Tetravalent uranium was then hydrolysed, leading to the precipitation of UO_{2+x} as the only crystalline phase. This study thus demonstrates that the hydrothermal conversion of actinide oxalates into oxides is an extremely versatile tool that can be implemented in a large variety of chemical systems, particularly in terms of the oxidation state of the cations initially present in solution.

Received 17th May 2024,
Accepted 23rd July 2024

DOI: 10.1039/d4dt01451k

rsc.li/dalton

1. Introduction

The fabrication of MOx-type nuclear fuels is currently based on powder metallurgy processes, and in particular, on the dilution of a UO_2-PuO_2 primary blend in uranium dioxide, enabling the final plutonium content to be easily adjusted.[1] This process leads to a heterogeneous distribution of cations within the final compound.[2,3] As part of the development of the next generation of nuclear reactors, however, fuel homogeneity needs to be improved, both to increase the plutonium content introduced and to enable the fuel to be reprocessed after its stay in the reactor. New preparation methods based on wet chemistry routes are therefore being studied.[4–6] They generally involve the complexation of actinides in solution to precipitate them within a single precursor, which is then converted to an oxide by heat treatment. In this context, a great deal of work has focused on the chemistry of actinide oxalates, which exhibit rapid precipitation kinetics and rich crystal chemistry.[4] However, the morphology of the resulting powders, as well as the presence of carbon in the final oxide samples, can degrade powder behaviour during the sintering stage.[7]

To limit these drawbacks, several authors have recently proposed the use of hydrothermal conditions to ensure the conversion of oxalates into oxides.[8–12] Several chemical systems have been explored, covering most of the actinides of interest to the nuclear fuel cycle (Th, U, Np, Pu), as well as some lanthanides such as Ce.[13] The temperature–pressure couple generated in the reactor initially ensures the decomposition of the organic fraction of the precursor, and then the tetravalent cations released into solution are hydrolysed, leading to a nanostructured hydrated oxide precipitate. This mechanism enables carbon to be removed efficiently, and the morphology of the resulting powders to be controlled, notably by adjusting the pH of the reaction medium. However, to date, most of this work has focused on tetravalent cations, and to our knowledge, no study has examined the behaviour of actinyl molecular cations, including UO_2^{2+} which is ubiquitous in nuclear fuel cycle chemistry.

However, the reduction of uranyl ions by organic compounds under hydrothermal conditions has already been reported under geological conditions. As an example, Nakashima *et al.* showed that uranyl ions were precipitated as

[a]*ICSM, Univ Montpellier, CEA, CNRS, ENSCM, Bagnols/Cèze, France. E-mail: nicolas.clavier@icsm.fr; Fax: +33 4 66 79 76 11; Tel: +33 4 66 33 92 08*
[b]*Université Grenoble Alpes, UAR CNRS 832, OSUG, 38041 Grenoble, France*
[c]*Institut Néel CNRS-UGA, 25 Avenue des Martyrs, 38042 Grenoble, France*
† Electronic supplementary information (ESI) available. See DOI: https://doi.org/10.1039/d4dt01451k

UO_{2+x} under mild hydrothermal conditions (T = 100–200 °C).[14–17] The reduction of uranyl ions was achieved in the presence of lignite, R_1R_2CHOH, or a secondary alcohol, *e.g.* propan-2-ol (eqn (1)). At a temperature of 200 °C, the authors reported that around 99.5% of the uranium initially present in the aqueous solution was precipitated, meaning that uranyl cations were quantitatively reduced under hydrothermal conditions.

$$UO_{2(aq)}{}^{2+} + [R_1R_2CHOH] \rightarrow UO_{2(s)} + 2H^+ \quad (1)$$

UO_{2+x} and $(U,An)O_{2+x}$ solid solutions (with An = Th and Np) were also obtained by Yamamura's group when using hydrothermal synthesis under supercritical water conditions,[18,19] while Hudry *et al.* achieved the reduction of uranyl ions into nanosized hyper-stoichiometric uranium dioxides using solvothermal conditions.[20,21] Building on these studies, it is thus possible to envisage the use of oxalates, not only as precipitating agents, but also as organic species able to quantitatively reduce uranyl ions, which could enable the development of an innovative synthesis route for $(U,An)O_2$ mixed oxides. With this in mind, the first part of this article examines the hydrothermal conversion of a mixture composed of uranyl and oxalate ions to produce uranium(IV) dioxide. A multi-parametric study was undertaken to assess the influence of various experimental parameters, such as pH, hydrothermal treatment duration, and oxalate concentration, on the nature and the physico-chemical properties of the samples obtained. In the second part, an *in situ* XANES study was carried out to monitor the uranium oxidation state within the hydrothermal cell during several conversion experiments. This novel approach provides a better understanding of the redox mechanisms involved in the reduction and conversion of uranium(VI) to UO_{2+x} by oxalate ions under hydrothermal conditions.

2. Materials and methods

2.1. Preparation of the samples

All the conventional chemicals were supplied by Sigma and were of analytical grade, while uranium was kindly provided by CETAMA. This latter was prepared as a solution of U(VI) in hydrochloric media by dissolving studtite $(UO_2(O_2)(H_2O)_2{\cdot}2H_2O)$ in 0.5 M HCl. The final uranium concentration was close to 0.1 M and was checked by ICP-AES (Spectro Arcos).

During the synthesis, the uranyl chloride solution was poured over a 0.5 M oxalic acid solution under stirring. An excess of 50% in oxalic acid was considered, taking into account the stoichiometry of eqn (2), which accounts for the quantitative precipitation of U(IV) oxalate. This choice is thus based on the assumption that the reduction of uranyl precedes its precipitation, as will be discussed later.

$$U^{4+} + 2C_2O_4{}^{2-} \rightarrow U(C_2O_4)_{2(s)} \quad (2)$$

In contrast to what was observed when studying the conversion of mixed uranium(IV) and cerium(III) oxalates,[12] no precipitation was observed here when mixing the reagents. Indeed, the solubility of uranyl oxalate is high[22] and qualified as "retrograde", the latter precipitating more efficiently as the temperature increases (typically from around 80 °C).[23] The pH of this solution, containing uranyl and excess oxalate, was initially close to 0.5 and was then adjusted between 0.5 and 2.0 using a commercial ammonia solution (16.5 M). The volume was then fixed at 15 mL with an aqueous solution at the desired pH values, and the reaction mixture was transferred to a Teflon-lined hydrothermal reactor (Parr, V_{tot} = 23 mL). The initial oxalic acid concentration in the reactor varied between 2.5×10^{-2} and 0.2 M, while that of uranium was set at 2.5×10^{-2} M. These values allowed us to explore a range of ratios $R = \frac{n_{oxalate}}{n_U}$ between 1 and 8. The reactor was then closed and heated to 250 °C, for a hydrothermal treatment duration ranging from 6 to 168 hours. Afterwards, the autoclave was taken out of the oven and then cooled down naturally on the benchtop before the reactor was opened. The final precipitate was recovered by centrifugation at 14 500 rpm, washed twice with deionized water and then with ethanol, and finally dried overnight in an oven at 90 °C.

At the same time, the supernatants and washing water were collected for analysis by ICP-AES, enabling post-conversion precipitation yields to be quantified. The intensities of the emission peaks at λ = 385.958 and 409.014 nm were considered for uranium concentration measurements. To calibrate the apparatus, a set of standard solutions was prepared, starting from 1000 ppm standard solutions purchased from SCP Science, with concentrations ranging from 0.5 to 15 ppm. The analysed solutions were diluted in order to present a concentration included in the calibration range and therefore to measure the concentration by interpolation.

2.2. Characterization of the precipitates

PXRD. Powder X-ray diffraction (PXRD) patterns were recorded using a Bruker D8 diffractometer equipped with a LynxEye detector adopting the Bragg–Brentano geometry and using Cu $K\alpha_{1,2}$ radiation (λ_1 = 1.54060 Å; λ_2 = 1.54439 Å). Data acquisitions were performed at room temperature, with 2θ varying from 5° to 90° with a step size of 0.01° and a total counting time of 205 minutes. Unit cell parameters were refined by the Rietveld method with GSAS-II software[24] using CIF files downloaded from the Inorganic Crystal Structure Database (# 246851) corresponding to UO_2.[25] Average crystallite sizes and phases quantification were also assessed when possible but proved to be only semi-quantitative.

SEM. Powder morphologies were observed using scanning electron microscopy. Powders were deposited on carbon adhesive tape, without any additional preparation. An FEI Quanta 200 scanning electron microscope equipped with an Everhart–Thornley Detector (ETD) and a back-scattered electron detector (BSED) was used to record micrographs at an acceleration voltage of 15 kV under high vacuum conditions (10^{-6} Pa).

2.3. *In situ* XANES experiments

X-ray absorption spectroscopy (XAS) analysis at the uranium U-L_3 edge was carried out on the CRG FAME beamline (BM30) at the European Synchrotron Radiation Facility (ESRF) in

Grenoble, France, which is specifically designed for the study of geochemical processes and offers the possibility to perform *in situ* experiments under hydrothermal conditions.[26] During our experiments, the storage ring was operated at 6 GeV with a nominal current of 200 mA in 7/8 + 1 mode. The incident energy was selected using a double-crystal Si(220) monochromator cooled with liquid nitrogen and surrounded by two Rh-coated mirrors for harmonic rejection. The second monochromator crystal was dynamically curved to focus the beam in the horizontal direction. The curvature of the first mirror was adjusted to collimate the beam in the vertical direction, thus optimizing energy resolution and photon flux on the sample, while the second mirror was curved to focus the beam in the vertical direction. Thanks to these elements, the beam spot on the sample was 210 × 100 μm^2 (HxV FWHM). Before measurements, the energy was calibrated using the absorption of a reference metallic Y-foil (K edge at 17038 eV).

During this study, an autoclave developed at the Néel Institute was used to record *in situ* XAS data under hydrothermal conditions.[27,28] This autoclave was designed so that pressure and temperature are independently controlled and regulated. Pressure was adjusted by injecting helium into the autoclave, while temperature was regulated using a resistive internal heating system arranged around the internal cell. Another key feature of this design is the confinement of the sample in an internal cell, avoiding contact with the high-pressure (HP) windows. In the case of our experiments, the windows used are made of beryllium. The signal can be detected in transmission mode, but also in fluorescence mode to access lower concentrations. This is the mode which was used during this work. The volume of the sample varied according to temperature and pressure conditions, which caused the pistons to move closer together or further apart. The sample volume can therefore be adjusted between 0.01 mL and 1 mL. In addition, the cell can be moved vertically, allowing the beam to interact with several discriminating zones during the experiments. For X-ray measurements, the cell and pistons are made of glassy carbon, which has very low absorption and very low chemical reactivity and is easy to machine.

To limit handling of radioactive samples on the FAME beamline, the uranium concentrations involved in these experiments were decreased to around 2.4 × 10^{-3} M, *i.e.*, about 10 times lower than that used under laboratory conditions. Approximately 300 μL of the reaction mixture, consisting of uranyl chloride solution and excess oxalic acid solution (R = 3), was introduced into the internal cell using a syringe, while the pH was adjusted to a value close to 1. The cell was then pressurized to 80 bars and heated. Fig. 1 highlights the typical fluorescence signal obtained when scanning vertically the thinned part of the cell, thus allowing us to discriminate between the signal coming from the solid precipitate and the one from the supernatant. Heating and X-ray beams might still induce some movements of the solid particles that can disturb the measurements. Nevertheless, this only results in variation of the signal intensity and not modifications of the XAS signal shape. As such, it does not preclude uranium redox speciation determination. Also, the possible photo-reduction of uranium(VI), well-known to occur during XPS experiments, should be considered under our operating conditions. From the initial tests performed on the U(VI) solution reference, this phenomenon was found to be absent at RT, but might take place when increasing temperature and pressure. This effect will be discussed further.

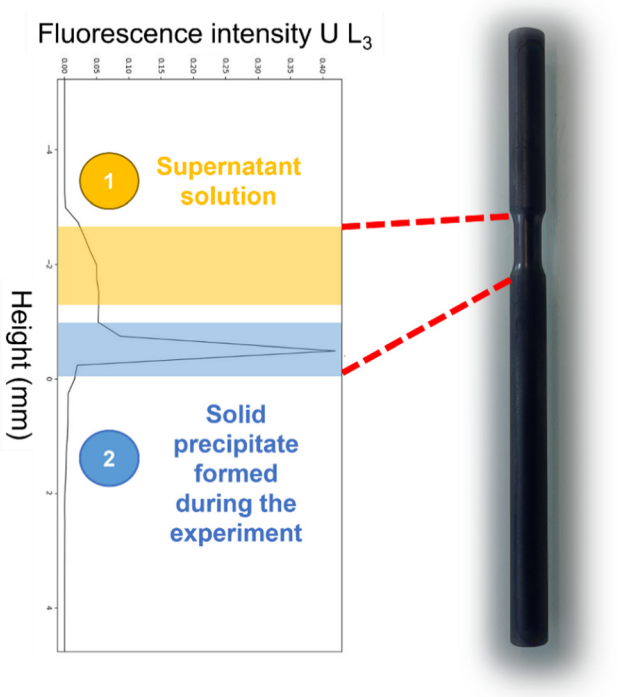

Fig. 1 Typical U-L_3 edge fluorescence signal obtained when scanning vertically the thinned part of the cell (pictured on the right), allowing the discrimination of solid and liquid phase signals on the ESRF's BM-30 FAME beamline. The area coloured in blue corresponds to the precipitate formed during the hydrothermal reaction, while the yellow zone corresponds to the supernatant.

3. Results

3.1. Multi-parametric study of the hydrothermal conversion

As evidenced in previous studies,[10–12] several experimental parameters can significantly affect the nature and the physico-chemical properties of the oxide phases obtained by hydrothermal conversion of oxalate precursors. Among these parameters, the temperature and duration of hydrothermal conversion, as well as the pH of the initial solution, have been identified as key variables. In addition, Manaud *et al.* have shown that when the conversion of uranium(IV) oxalate was carried out at a temperature of 250 °C, the O/U ratio of the final UO_{2+x} uranium oxide reached a minimum value of around 2.13.[11] Since the present study aimed to reduce uranyl cations, a temperature of 250 °C was chosen for all the experiments. These conditions also correspond to those used by Nakashima *et al.* when studying the hydrothermal reduction of U(VI) by organic matter.[14,15,17]

3.1.1. Effect of the initial pH. The first experimental parameter investigated was the pH of the starting solution containing uranyl and oxalate ions. This latter was typically set between 0.5 and 2.0. At the same time, the hydrothermal duration was kept at 24 hours, and a R = 3 ratio was considered, which corresponds to a 50% excess of oxalic acid when considering the equilibrium described in eqn (2). At a value of 0.5, which corresponds to the initial pH of the reactant mixture, no precipitate was obtained either before or after the hydrothermal treatment. The reactor content remained in the form of a light yellow solution, which suggests that, after decomposition of the oxalates during hydrothermal treatment, uranium (VI) remained in solution as the free uranyl cation UO_2^{2+}(aq.), without having been reduced or precipitated. Conversely, for an initial pH between 0.8 and 1.4, a dark (black to brown) precipitate was recovered, while for higher pH values, an abundant and brown-yellow solid was obtained.

As a first step, ICP-OES measurements were carried out on the supernatants and washing water, collected after hydrothermal conversion, to quantify uranium precipitation yields (Table 1). These results show an increase in the precipitation yield with the pH of the solution, in good agreement with the visual inspection of the reactors just after the hydrothermal treatment. For starting pH between 0.8 and 1.2, around 75% of the uranium introduced was precipitated, while precipitation became quantitative at pH = 1.4. It should be noted that the precipitation yields measured for pH values below 1 are in line with the data reported for the hydrothermal conversion of uranium(IV) oxalate by Manaud *et al.* (approx. 72%), which could be seen as a first indication of the reduction of uranium(VI) before its precipitation.[11]

The powders obtained after hydrothermal treatment were then characterized by PXRD (Fig. 2a). It can be seen that the samples obtained at different pH values all have different structures. At pH = 0.8, the characteristic fluorite-type structure of UO_{2+x} (containing mainly tetravalent uranium) is recovered as a pure phase, while at pH = 1, the formation of UO_{2+x} and α-U_3O_8, consisting of a U(V)/U(VI) mixture, is obtained. From pH = 1.2, the precipitate is composed of α-U_3O_8 and a uranyl oxide hydroxide called meta-schoepite, with the formula $(UO_2)_8O_2(OH)_{12}{\cdot}10H_2O$.[29]

Table 1 Variation in the uranium precipitation yields $\rho(U)$, expressed in %, after hydrothermal treatment as a function of several operating parameters: initial pH, initial oxalate concentration with $R = \frac{n_{oxalate}}{n_U}$, and hydrothermal treatment duration. The uncertainty attached to the precipitation yields is about ± 2%

Effect of the initial pH (T = 250 °C; t = 24 h; and R = 3)							
pH	0.8	1.0	1.2	1.4	1.6	2.0	
$\rho(U)$ (%)	78	78	75	99	95	93	
Effect of oxalate concentration (T = 250 °C; t = 24 h; and pH = 0.8)							
R ratio	1	2	3	4	6	8	
$\rho(U)$ (%)	0	5	78	86	94	97	
Effect of treatment duration (T = 250 °C; pH = 0.8; and R = 3)							
Holding time (h)	6	14	18	24	48	72	168
$\rho(U)$ (%)	27	40	55	78	75	98	95

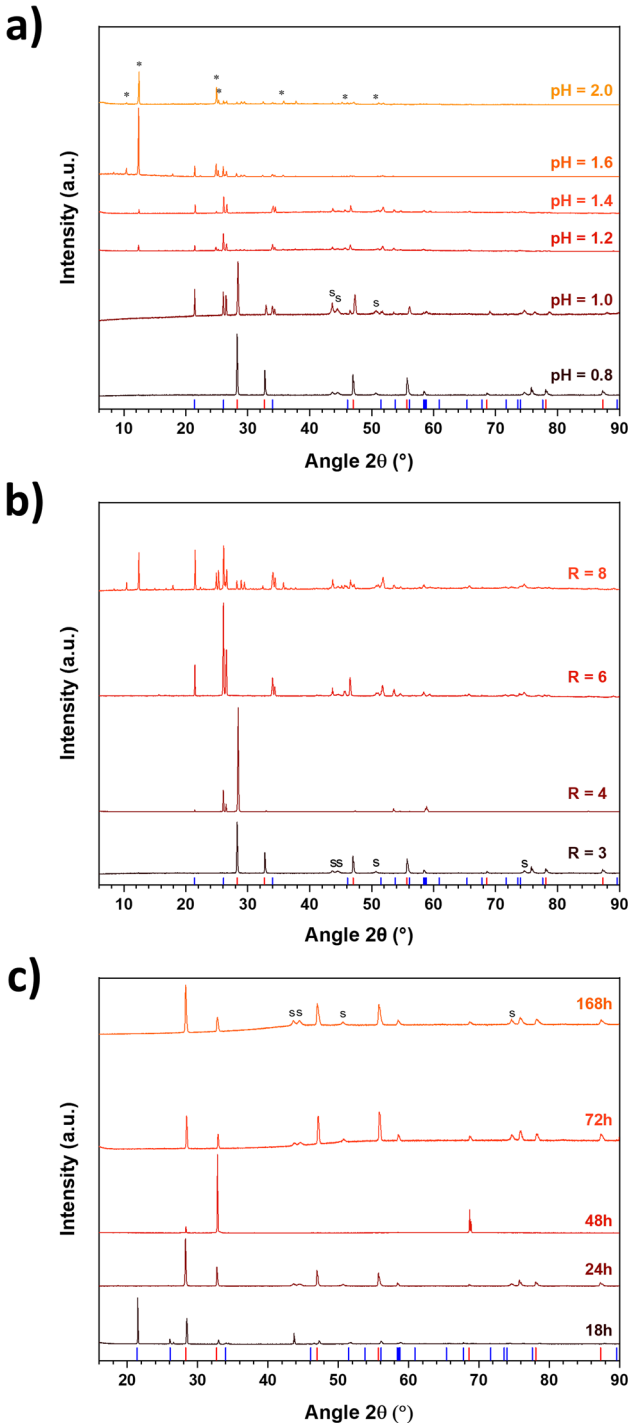

Fig. 2 PXRD patterns of the samples obtained from the hydrothermal conversion of U(VI) oxalate as a function of initial pH (a), oxalate concentration (b), and treatment duration (c) (T = 250 °C). PXRD line positions for α-U_3O_8 (blue bars),[30] UO_2 (red bars),[31] and meta-schoepite (black stars)[29] are supplied for comparison, while 's' accounts for the sample holder signal (austenite, PDF 00-023-0298).

These samples were finally observed by SEM to characterize their morphology (Fig. 3). At pH = 0.8, UO_{2+x} single crystals in the form of bipyramids with a square base and a size of around 5 μm were prepared. This morphology is similar to

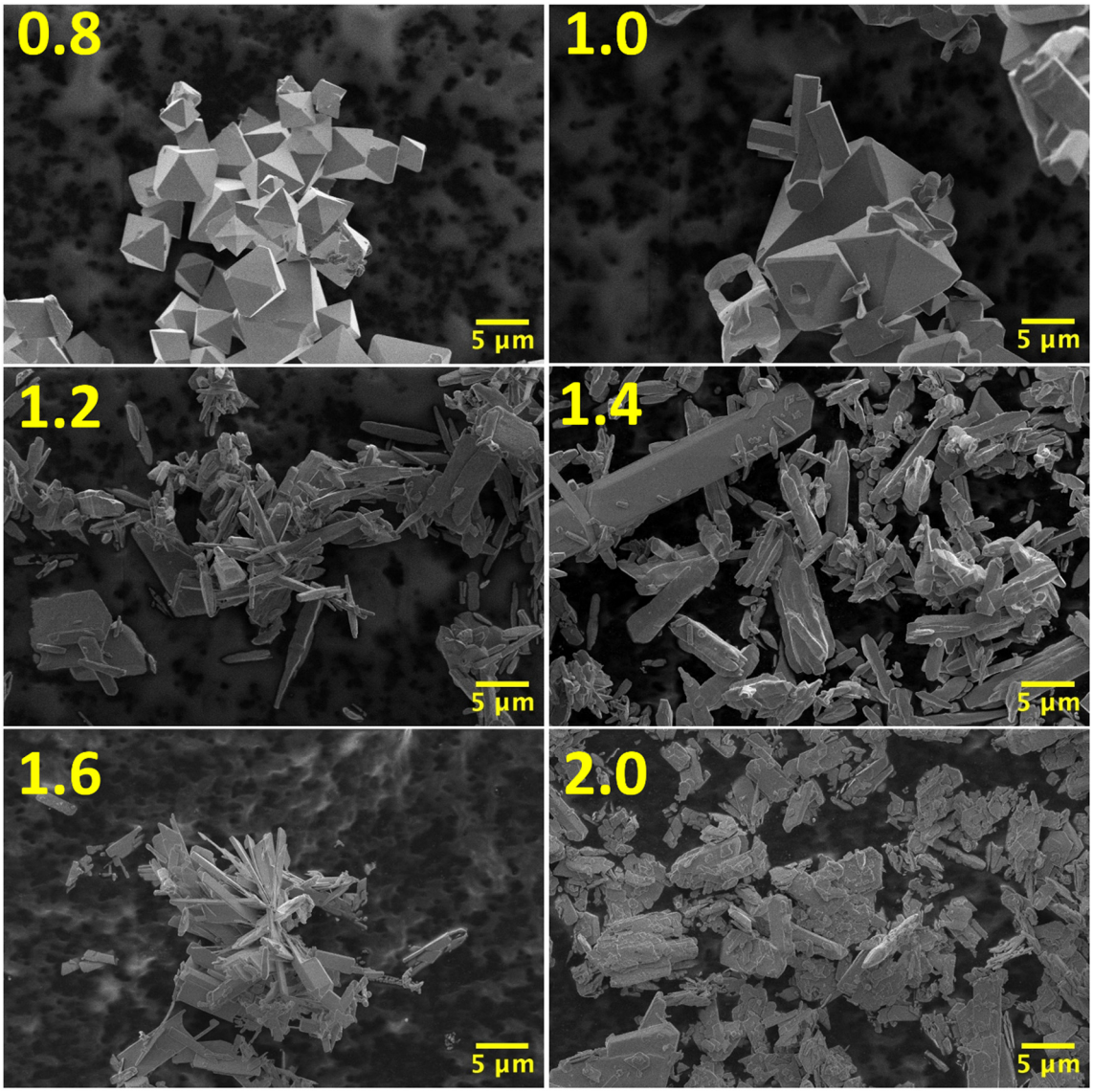

Fig. 3 SEM (SE mode) micrographs recorded for the samples obtained after the hydrothermal treatment of uranyl oxalate (T = 250 °C, holding time = 24 hours, and R = 3) with various starting pH values (indicated in yellow in the upper left corner of the images).

that frequently observed in crystals of CaF_2 [32] or UO_2 [33] isotypes. At pH = 1, the same UO_{2+x} bipyramids were obtained along with α-U_3O_8 hexagonal rod crystals. Under both conditions, the formation of single crystals was probably related to a slow reduction of uranium(VI) in solution before precipitation, favouring crystal growth over nucleation. Lastly, for pH values above 1, the morphology obtained can be described as heterogeneous agglomerates of needle-like or plate-like crystals, as observed by Riba *et al.* during their synthesis of meta-schoepite.[34]

3.1.2. Effect of the starting oxalate concentration. To improve the uranium reduction/precipitation yield, a second series of experiments involved varying the value of the molar ratio $R = \frac{n_{oxalate}}{n_U}$ within the starting mixture, while keeping other parameters constant, *i.e.*, T = 250 °C, t = 24 hours and pH = 0.8. Oxalate was previously introduced in a 50% excess compared with the stoichiometric conditions of eqn (2), corresponding to R = 3. In this new series of experiments, the initial oxalate concentration therefore varied between 0.025 M (R = 1) and 0.2 M (R = 8), while the uranium concentration remained unchanged. Moreover, the pH of the solution was set to 0.8 to obtain UO_{2+x} as a single phase. For a value of R = 1, no precipitate was recovered from the reactor after hydrothermal treatment. Increasing the R value then led to an enhancement in the precipitation yield, going from 5 ± 2% for R = 2 to 97 ± 2% for R = 8 (Table 1).

A series of PXRD analyses then led to the identification of the phases formed during the hydrothermal process (Fig. 2b). For R = 2, no characterization of the solid could be carried out due to the small quantity of material obtained. Conversely,

and as shown previously, only the characteristic PXRD lines of the fluorite-structure phase were observed for R = 3. As the R ratio increased, however, the structure of the samples evolved. Indeed, for R = 4, although the peaks of the fluorite structure remained the main feature, an additional signal characteristic of α-U_3O_8 appeared, which evidences an incomplete reduction of U(VI) to U(V) and then to U(IV). For R = 6, a pure α-U_3O_8 phase was obtained, meaning once again that uranium reduction was only partial and in this case did not even lead to the formation of uranium(IV). Finally, for R = 8, α-U_3O_8 was still detected along with an unidentified phase. This latter is characterized by several diffraction lines, especially at 10.5, 12.4, 24.9 and 25.3° (2θ), which do not match with the reference patterns of uranyl oxalates, schoepite/meta-schoepite or uranyl hydroxide reported in the databases. This signal is thus most probably related to an unknown uranyl oxo-hydroxide stabilized by the use of hydrothermal conditions.

3.1.3. Effect of hydrothermal treatment duration. The last series of experiments focused on the impact of hydrothermal treatment time on the conversion of the initial reaction mixture. For this purpose, the hydrothermal treatment temperature was maintained at 250 °C, the pH of the initial solution at 0.8 and the oxalate excess at 50% (R = 3). The duration of the hydrothermal treatment varied from 6 to 168 hours. Uranium precipitation yields (Table 1) increased significantly with the duration of hydrothermal treatment, with precipitation becoming quantitative for durations greater than 72 hours. This once again backs up the hypothesis of a slow U(VI) reduction kinetics.

From a structural point of view, after 18 hours of hydrothermal treatment, the characteristic PXRD lines of α-U_3O_8 and UO_{2+x} were observed (Fig. 2c), meaning that uranium(VI) reduction has already begun at this stage. For conversion durations longer than 24 hours, the powders obtained showed only the characteristic peaks of the fluorite structure typical of UO_{2+x}. It should be noted that for a conversion time of 48 hours, the PXRD pattern shows all the peaks of the fluorite structure, but with unusual intensity ratios. Insofar as none of the diffraction peaks observed on all the other diffractograms highlight irregular intensities, this preferential orientation probably does not reflect a preferred crystal growth direction and might result from an experimental artefact coming from the synthesis process or from sample preparation for PXRD analysis.

3.2. *In situ* XANES monitoring of the uranium oxidation state

3.2.1. Uranium behaviour in solution. To gain a better understanding of the redox mechanisms involved in the reduction and conversion of uranium(VI) to UO_{2+x} by oxalate ions under hydrothermal conditions, *in situ* XANES analyses were carried out on the BM30-FAME beamline at the ESRF synchrotron. This technique is particularly well suited for the analysis of actinides, which can often be stabilized in multiple oxidation states.[35,36] The first series of experiments focussed on the behaviour of uranium in solution, *i.e.*, in the upper part of the cell (zone "1" in Fig. 1). In addition, two reference spectra were recorded upstream of these experiments for comparison (spectra are supplied as supplementary material, Fig. S1†). The first one came from a U(VI) solution in 1.2 M HCl (C_U = 2.4 × 10^{-3} M) and was recorded at 250 °C as a reference for the initial system containing UO_2^{2+} cations. The second reference was an uranium(IV) hydrochloric solution with an identical concentration, which was measured at room temperature to slow down U(IV) hydrolysis and hinder the formation of a precipitate.[37] It is important to note that these solutions did not contain oxalate ions, which would cause precipitation of $U(C_2O_4)_2{\cdot}nH_2O$ in the case of the uranium(IV) reference.[38] From these measurements, it can be seen that the uranium(IV) reference spectrum exhibits an absorption edge shifted towards low energies compared with that containing uranium (VI). The inflection points are located at 17 169.6 eV and 17 168.1 eV, while the white line (corresponding to the absorption maximum) is located at 17 175.1 eV and 17 174.1 eV for U(VI) and U(IV) references, respectively. The two spectra also show a different profile for energies above 17 180 eV, which corresponds to the first oscillations of the EXAFS spectra. This can be easily explained by the distinct environments of the uranium atom in the UO_2^{2+} and U^{4+} forms, especially due to the two shorter U–O multiple bonds characteristic of the uranyl unit.[39,40]

XANES spectra were first recorded continuously in the upper part of the hydrothermal cell, corresponding to the supernatant, during the hydrothermal conversion of a uranyl oxalate mixture at 250 °C for 18 hours (R = 3, pH ∼ 1). This led to the acquisition of more than thirty spectra, from which the data presented in Fig. 4 are derived. Fig. 4a shows a significant decrease in the absorption at the U-L_3 edge over time, confirming that uranium precipitates during hydrothermal treatment and settles at the bottom of the cell (zone 2 in Fig. 1). Fig. 4b presents the same spectra, but after normalization of the intensity using the Athena software.[41] A shift in the absorption edge towards lower energies can then be observed. Indeed, the initial spectrum shows an inflection point at 17 170.2 eV and a white line at 17 175.7 eV, while the final one exhibits an inflection point at 17 168.2 eV and has its white line located at 17 174.7 eV. As the energy was initially calibrated using a reference Y-foil, this modification is likely to come from a chemical transformation in the solution. Based on the references described above, this shift can easily be attributed to the reduction of uranium in solution during hydrothermal conversion. This hypothesis is also backed up by the data reported in the literature, several authors having recorded XANES spectra at the L_3-edge of compounds incorporating uranium in various oxidation states.[42–45] The profile of the spectrum after 17 180 eV also strongly differs between the initial and final spectra. Indeed, the blue spectrum in Fig. 4b does not show any oscillation between 17 210 and 17 220 eV, and its intensity decreases steadily after the white line. As explained previously, such evolution reflects the existence of modifications in the uranium coordination mode, which is also in line with the reduction of the UO_2^{2+} uranyl molecular ion to U^{4+} in solution.

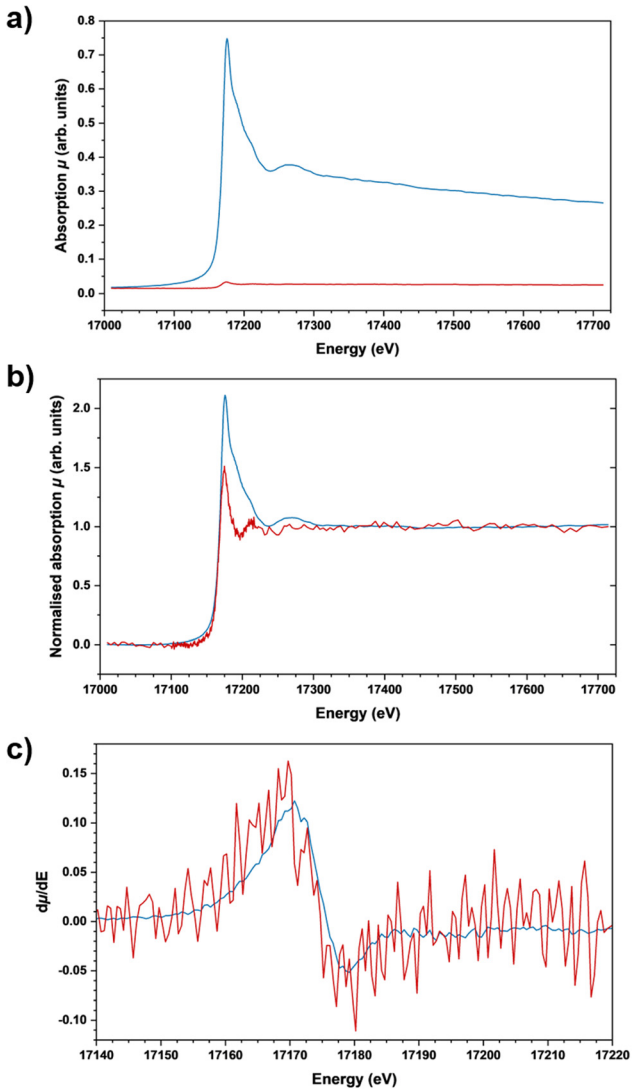

Fig. 4 Evolution of the XANES spectra at the U-L_3 edge (fluorescence mode) of a solution containing uranyl and oxalate ions (R = 3 and pH ~ 1) during hydrothermal treatment at T = 250 °C. The blue spectra were recorded at t = 0 and the red spectra at t = 18 h. Raw absorption data are presented in (a), whereas post-edge normalisation was performed in (b). Derivative curve used for the determination of inflection points and the white line position (c).

Conventionally, XANES data are processed in the form of linear combinations of reference spectra, each one corresponding to a compound incorporating the element of interest present in a different oxidation state or in a different geometrical environment. Such methodology is now widely applied, among other cases, to U-based oxides, for which the distribution of the oxidation states of uranium is derived from the linear combination of several spectra, such as those of UO_2, U_4O_9 and U_3O_8.[46] With the same objective, the intensity of all the spectra collected in the supernatant during this study was normalised, before they were adjusted by linear combination. However, in this particular case, it was not possible to use the measured U(IV) and U(VI) references, as they are free from oxalate ions for stability purposes. We then chose to consider our spectra as linear combinations of the initial and final states, with the hypothesis that these latter reflect the contributions of uranium(VI) and uranium(IV), respectively, in the solution during the hydrothermal treatment.

This assumption was validated by comparison with the reference spectra (see Fig. S2† in the supplementary material). The initial spectrum shows a similar absorption threshold to the U(VI) reference, indicating that at the very beginning of the hydrothermal treatment, only uranium(VI) was present in the solution. The final spectrum shows a noisy signal due to the low concentration of uranium in solution following hydrothermal conversion. Nevertheless, as evidenced before, it can be seen that the absorption threshold shifts towards that of the U(IV) reference, suggesting at least partial reduction of uranium remaining in solution.

As a result of the linear combination fitting, Fig. 5 presents the evolution of the fraction of the initial U species in solution, assumed to be U(VI), possibly in the form of free UO_2^{2+} cations (see Fig. S3† in the supplementary material for an example of linear combination fitting). In the reaction medium, a rapid decrease is observed over time, which can be explained by the reduction of uranium(VI) in solution. As such, 70% of the initial U(VI) content was found to be reduced after only 5 hours of hydrothermal treatment.

To complement this observation and to monitor uranium (IV) precipitation, a second set of experiments was carried out at 200 °C to slow down the kinetics. The fluorescence intensity of uranium was then continuously measured at a fixed energy of 17.5 keV, *i.e.*, above the U-L_3 absorption edge, for about 2 hours (Fig. 6). Once again, it can be seen that the fluorescence intensity of uranium in solution decreased rapidly

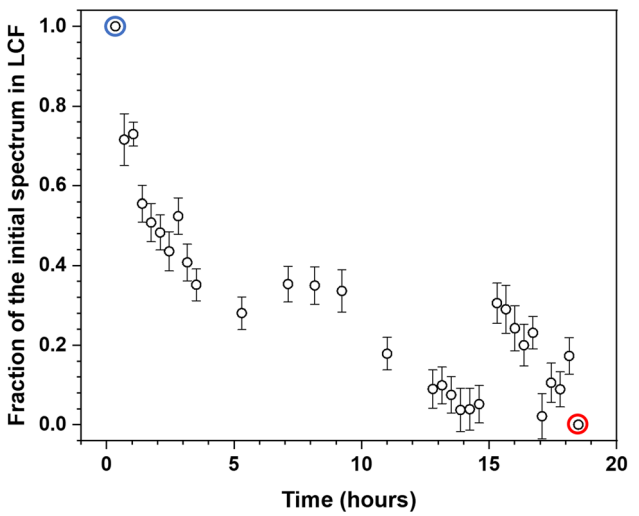

Fig. 5 Variation of the fraction of the initial spectrum in the linear combination fit (LCF) of XANES spectra at the U-L_3 edge acquired during the hydrothermal treatment of a solution containing uranyl and oxalate ions (R = 3 and pH ~ 1) at T = 250 °C. The datapoints corresponding to the first and last spectra recorded are circled in blue and red, respectively.

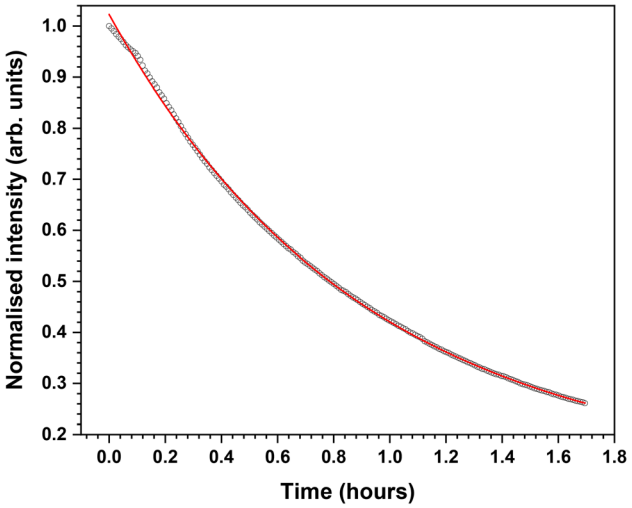

Fig. 6 Evolution of the normalised fluorescence intensity of uranium measured at 17.5 keV in solution, illustrating uranium precipitation (T = 200 °C).

(only 40% of the initial intensity was recorded after only 1 hour of hydrothermal treatment), indicating that uranium, initially present in solution, precipitated at the bottom of the cell. Moreover, this curve can be fitted using a decreasing exponential function ($R^2 \approx 0.9995$), in the following form:

$$\frac{I}{I_0} = 0.899 \times \exp\left(\frac{-t}{3250}\right) + 0.124 \quad (3)$$

Even if this measurement remained only qualitative, it was sufficient to show that the precipitation kinetics follows a first-order kinetic law. The curve also shows a similar profile to the reduction kinetics evidenced in Fig. 5. Although the two experiments were not carried out at the same temperature, their results confirm that uranyl cations are reduced in solution, probably by oxalates or their decomposition products, and that the resulting tetravalent uranium precipitates very rapidly.

3.2.1. Uranium behaviour in the precipitate. A similar approach was applied to the study of the solid phase precipitated in the lower part of the cell during the hydrothermal treatment, corresponding to the zone labelled "2" in Fig. 1. Once again, XANES spectra at the U-L_3 edge were acquired continuously during the hydrothermal conversion of U(VI) oxalate, performed at T = 250 °C for 18 hours (R = 3, pH ~ 1). Fig. 7a presents three representative spectra acquired on the solid during hydrothermal treatment. Since no normalization was performed, a slight variation in the absorption could be observed over time. However, this variation is not significant and can probably be attributed to grain movements in the cell, possibly induced by the incident X-ray beam. To suppress this variation, the spectra were normalised, as presented in Fig. 7b, while the positions of the energy of the inflection points and white lines of the three spectra are compiled in Table 2. No shift in the absorption edge was observed, indicating that no change in the uranium oxidation state occurred in the solid phase during hydrothermal treatment. In addition, these three spectra showed a different white line position and profile compared with the initial spectrum recorded in the supernatant (Fig. 4). As a result, uranium present in the precipitate was tet-

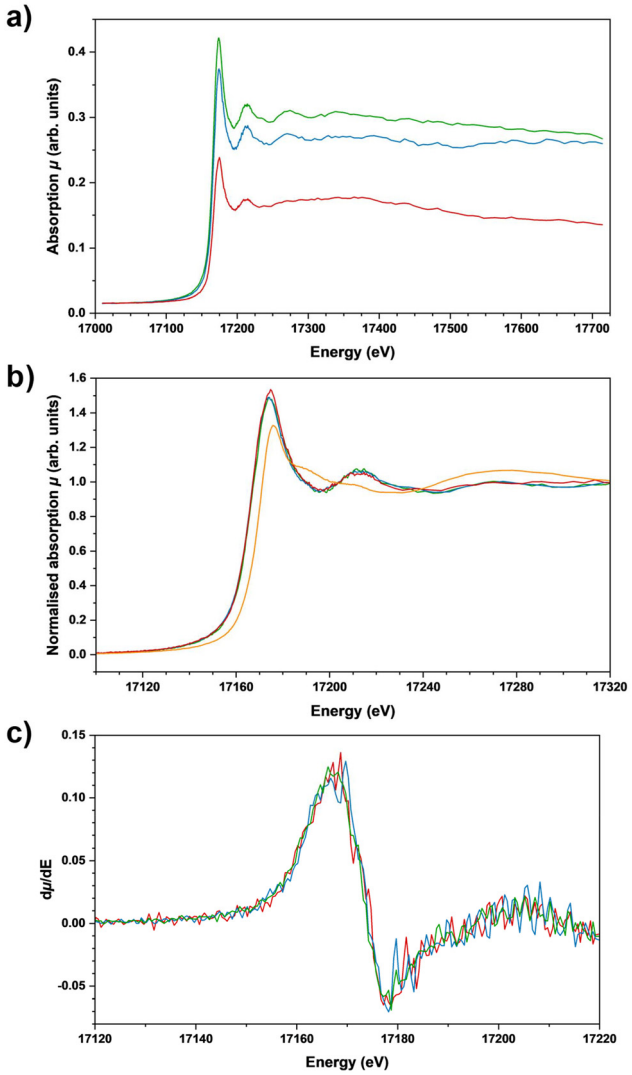

Fig. 7 (a) X-ray absorption spectra at the uranium L_3 edge (fluorescence mode) acquired in the precipitate formed during hydrothermal conversion: t = 0 (blue), t = 10 hours (green) and t = 18 hours (red). (b) Same data after the normalisation of intensity. The data recorded in the solution at t = 0 are presented in orange for comparison. (c) Derivative curves.

Table 2 Energy positions of the inflection points and white lines for the XANES spectra of interest for the solution and the solid

	Solution, t = 0	Solid, t = 0	Solid, t = 10 hours	Solid, t = 18 hours
Inflection point (eV)	17 170.2	17 168.2	17 167.2	17 168.2
White line (eV)	17 175.7	17 174.2	17 174.2	17 174.7

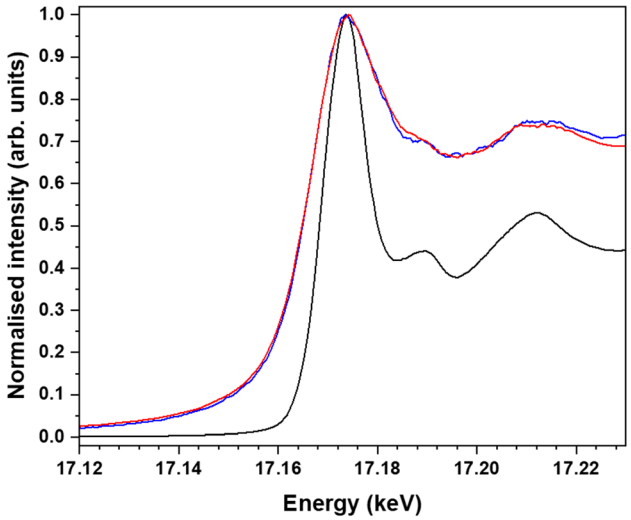

Fig. 8 Comparison of XANES spectra at the U-L_3 edge of final precipitates obtained from the conversion of a uranyl solution and an excess of oxalate (U(VI) system) (in blue), from the conversion of uranium(IV) oxalate precipitate (U(IV) system) (in red) and from a reference spectrum of UO_2 acquired by HERFD-XANES (in black).

ravalent from the outset, and its oxidation state did not vary during hydrothermal treatment. These results also confirmed that the uranium present in zone 2 of the hydrothermal cell very quickly showed a different complexation from that of the uranyl ion in solution.

Lastly, the final spectrum recorded for the precipitate after 18 hours of treatment was compared with two spectra of the reference in order to identify the nature of the precipitate formed during hydrothermal conversion (Fig. 8). The first one came from a UO_2 sample measured in HERFD-XANES mode (in black), while the other was collected from a sample obtained by hydrothermal conversion of uranium(IV) oxalate (in red), which is now well-known to systematically yield UO_{2+x}.[11] Even if differences in resolution arise from the use of the high resolution mode for one of the samples, the typical features of the three spectra remain identical. As such, the white line was measured at 17 173.7 eV for UO_2 in HERFD-XANES, whereas that of the spectrum from the oxide obtained by conversion of uranium(IV) oxalate was found at 17 174.1 eV. These values are very close to those reported in Table 2 for the solid obtained in the course of this work. In addition, the first EXAFS oscillations of the three spectra shown are observed at identical energies, *i.e.*, 17 189.7 and 17 211.7 eV. Taken together, all these observations confirm the formation of UO_{2+x} during the hydrothermal treatment of the uranium(VI)–oxalate mixture.

4. Discussion

The multi-parametric study first conducted during this work clearly showed that it is possible to quantitatively precipitate UO_{2+x} samples from the hydrothermal reduction of mixtures composed of uranyl ions and oxalic acid, without the addition of any supplementary reducing agent. The pH of the initial reaction mixture had a drastic influence on the nature of the precipitate obtained. Indeed, three phases incorporating uranium in three different oxidation states were obtained within a narrow range of 0.4 pH units, *i.e.*, UO_{2+x} at pH = 0.8 (U(IV)), U_3O_8 at pH ≥ 1 (U(V) and(VI)), and meta-schoepite at pH ≥ 1.2 (U(VI)). As these results showed that decreasing the pH promoted the reduction of uranium, structural refinements using the Rietveld method were carried out to estimate qualitatively the evolution of the O/M ratio in UO_{2+x} phases. The calculated unit cell parameters are reported in Table 3. In line with the previous observations, the lattice parameter of fluorite-type phases increased when using a more acidic medium. This trend suggests a lower O/M value when decreasing the pH value. Indeed, it is well known that hyper-stoichiometry in UO_{2+x} is accompanied by a decrease in the lattice parameter of the structure,[47] in agreement with the variation of the ionic radius of uranium, which decreases from 1.00 Å for U(IV) down to 0.88 Å for U(V).[48]

The modification of the pH was also linked with significant variations in the precipitation yield values. Indeed, the uranium precipitation was not quantitative after 24 hours of hydrothermal treatment when a UO_{2+x} fluorite-type phase was obtained, *i.e.* for pH = 0.8 (as a single phase) or pH = 1.0 and 1.2 (as a mixture with U_3O_8), while it reached almost 100% when meta-schoepite was prepared at pH > 1.2. This observation could be justified by both thermodynamic and/or kinetic considerations. Indeed, using such acidic media could partly hinder U(IV) hydrolysis following the reduction step, thus affecting the precipitation of UO_{2+x}. Nevertheless, increasing the conversion time made the precipitation yield quantitative after 72 hours of treatment at pH = 0.8, with more than 95% of U(VI) initially introduced in the reactor being turned into UO_{2+x} precipitate. As such, the reaction yield appeared to be mainly driven by kinetics, with the uranium reduction from UO_2^{2+} to U^{4+} acting as a limiting step. Indeed, when U(IV)/U(VI) phases were observed (pH ≥ 1.2), no complete reduction of uranium was required upstream of the precipitation process,

Table 3 Unit cell parameters calculated by Rietveld refinements of the PXRD pattern of UO_{2+x} formed by the hydrothermal conversion of a U(VI)–oxalate mixture (T = 250 °C and R = 3)

Effect of the initial pH		
Initial pH	a (Å)	V (Å^3)
0.8	5.4674 ± 0.0001	163.44 ± 0.01
1.0	5.4332 ± 0.0003	160.38 ± 0.03
Effect of treatment duration		
Time (hours)	a (Å)	V (Å^3)
18	5.4404 ± 0.0004	161.02 ± 0.03
24	5.4674 ± 0.0001	163.44 ± 0.01
72	5.4682 ± 0.0003	163.51 ± 0.02
168	5.465 ± 0.001	163.17 ± 0.05

resulting in quantitative uranium precipitation after only 24 hours of treatment. As the aim of this work was to produce UO_{2+x} oxides from the hydrothermal reduction of U(VI)/oxalate mixtures, we tried to enhance the precipitation of uranium by accelerating the reaction kinetics. Two approaches were then used, *i.e.*, increasing the amount of oxalic acid and/or the hydrothermal treatment duration.

Although the precipitation yield increased with the value of the R ratio, the structure of the precipitate differed, with UO_{2+x} being obtained as a pure phase only for $R = 3$. For higher values of R, uranium(VI) appeared to be only partially reduced. This hypothesis was corroborated by the decrease of the unit cell volume of the UO_{2+x} phases obtained for $R = 3$ ($V = 163.43 \pm 0.01$ Å) and $R = 4$ ($V = 160.55 \pm 0.03$ Å), meaning that uranium was oxidized to a greater extent in UO_{2+x} as the oxalate concentration increased.[14] One hypothesis to explain this phenomenon is that anionic uranyl oxalate complexes could be stabilized in solution by a significant excess of oxalate (*e.g.*, for $R = 8$, the molar excess of oxalate was 300% compared to the stoichiometric conditions of eqn (2)). This parasitic secondary reaction could then lead to the precipitation of uranyl cations by the oxalate ligands as the R ratio increases, followed by partial reduction of uranium within the solid phase. This would explain the formation of U_3O_8 for $R \geq 4$, and the precipitation of a uranyl-containing phase for $R = 8$.

When varying the duration of the hydrothermal treatment (with $T = 250$ °C, pH = 0.8, and $R = 3$), Rietveld refinements were performed on PXRD data to extract unit cell parameters, as gathered in Table 3. Examples of fit and extensive refinement results are provided as supplementary data (Fig. S4 and Table S1†). These results show a significant increase of the unit cell volume with time, going from 161.02 ± 0.03 Å^3 after 18 hours to 163.44 ± 0.01 Å^3 after 24 hours. For conversion times greater than or equal to 24 hours, a plateau was reached around a value close to the volume reported in the literature for $UO_{2.00}$ (163.49 Å^3).[25] In parallel, evaluation of the precipitation yields showed quantitative precipitation of uranium in a UO_{2+x} phase. Such an evolution once again confirmed the progressive reduction of uranium(VI) throughout hydrothermal treatment, the latter being probably the limiting step in the overall kinetics of hydrothermal conversion.

In line with these conclusions, *in situ* XANES experiments allowed us to track the behaviour of uranium in solution. As expected from the characterization of the precipitates formed under various operating conditions, uranyl cations initially present in solution were found to be reduced in solution, following first-order kinetics. Still, several redox reactions can be considered for the reduction of U(VI) by oxalate ions. Eqn (4) should apply if we consider that oxalates are rapidly decomposed by the temperature and autogenous pressure imposed by hydrothermal conditions. This corresponds to the reaction between the UO_2^{2+}/U^{4+} couple of standard potential $E° = 0.327$ V/ESH[49] and the CO_2/CO couple ($E° = -0.53$ V/ESH[50]). In this case, carbon monoxide acts as a reducing agent for uranyl cations. However, it is also possible, if oxalate ions are introduced in large excess, which was the case in this study, for uranyl ions to be reduced in solution by oxalic acid, in which case eqn (5) should be considered ($E° = -0.49$ V/ESH for $CO_2/H_2C_2O_4$[51]). It is also possible that these two reduction processes are taking place simultaneously.

$$UO_2^{2+} + CO + 2H^+ \rightarrow U^{4+} + CO_2 + H_2O \quad (4)$$

$$UO_2^{2+} + H_2C_2O_4 + 2H^+ \rightarrow U^{4+} + 2CO_2 + 2H_2O \quad (5)$$

From a global point of view, the reduction reaction appeared to proceed way faster in the hydrothermal cell used during synchrotron measurements than under laboratory conditions. This difference could be partly related to the modification of the operating conditions, particularly in terms of uranium concentration (due to safety restrictions) and pressure (which is close to 60 bars in the conventional reactor, and was increased to 80 bars in the XAS cell). As such, it is possible that the competition between the reactions described by eqn (4) and (5) evolved differently in the two experimental setups, the latter being disadvantaged with an increase of pressure. Also, a possible contribution of uranium(VI) photo-reduction cannot be completely ruled out. Indeed, the spontaneous reduction of U(VI) under X-ray beams has been widely described, especially during XPS measurements.[52,53] Nevertheless, in our case, no reduction of the U(VI) reference solution was observed, although the measurement was made at room temperature, and on a shorter timescale compared to the 18 hour long experiment. Also, uranyl species were reduced under laboratory batch conditions, meaning that even if X-ray beams could have a catalytic effect, they are not required to complete the reaction. Nevertheless, these first results only provide a qualitative approach to the redox behaviour of uranium in solution under hydrothermal conditions. Further experiments are then required to properly and quantitatively determine the associated kinetics and possibly assess other parameters such as kinetic constants and activation energies.

Once uranium(VI) was fully reduced into uranium(IV), precipitation quickly occurred, leading the solid phase to settle at the bottom of the reactor. Scanning this second location showed that not only the oxidation state of uranium was modified, but also its complexation, as shown by the first oscillations of the EXAFS spectra. This is easily explained by the decomposition of oxalates under the effect of temperature and autogenous pressure and the hydrolysis of U(IV) under the pH conditions considered. As such, the XAS spectra recovered from the solid fraction in the reactor perfectly match those of UO_{2+x}. Also, the white line position did not vary during the hydrothermal treatment, meaning that the local environment of the uranium atoms remained similar. As such, no signal corresponding to the $U(OH)_4$ species was observed. In the literature, some authors have questioned the equilibrium to be considered for the formation of hydrated oxide from the U^{4+} cation in solution[54] and proposed the following two equilibria:

$$U^{4+} + 4OH^- \leftrightarrow U(OH)_4 \rightarrow UO_2 \cdot nH_2O \quad (6)$$

$$U^{4+} + 4OH^- \rightarrow UO_2 \cdot nH_2O + (2-n)H_2O \quad (7)$$

Our observations therefore tend to show that under the conditions studied, the precipitated phase is directly a hydrated

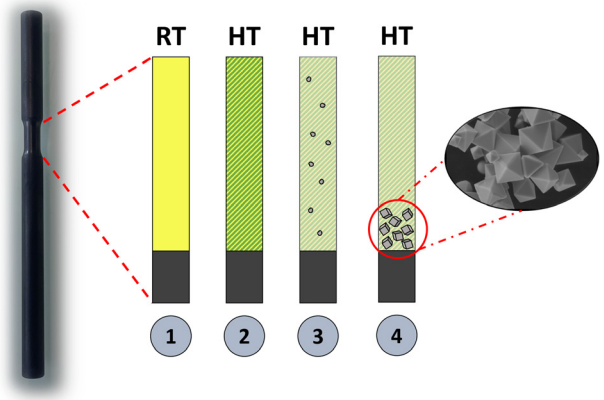

Fig. 9 Schematic representation of the hydrothermal conversion of a uranyl solution into hydrated uranium(IV) dioxide.

oxide. The overall equilibrium to be considered should then be that of eqn (7). Nevertheless, it is important to point out that few experimental data exist for the hydroxide form, probably due to its metastable nature. As such, the XAS spectra of UO_2 and $U(OH)_4$ are possibly close. The most stable U–OH distance, however, has been calculated to be 2.087 Å,[55] which is very distinct from the U–O bond length in uranium(IV) dioxide (2.368 Å).[25] A similar coordination is then expected, although with different bond lengths that could cause a sufficient shift in the first oscillations of the EXAFS spectra to distinguish the two forms. Also, the $U(OH)_4$ species could still be formed as a potential reaction intermediate, existing only for a short time, for example as colloids in solution quickly aggregating into oxide solid precipitate. This mechanism is now well-known in the case of An(IV) chemistry[56] and should be envisaged here.

Indeed, the *in situ* XAS data collected during this work provide a better understanding of the mechanisms underlying the reductive hydrothermal conversion of a uranyl solution to oxide, in the presence of oxalate ions (Fig. 9). At room temperature, and unlike the case of An(IV), the mixture of uranyl ions and oxalic acid leads to a homogeneous solution, owing to the high solubility of U(VI) oxalates (①). The formation of a uranium(VI) oxalate was not observed either when hydrothermal conditions were reached, which means that the increase in temperature and pressure very rapidly leads to the decomposition of the oxalate entities and to the reduction of U(VI) to U(V), and then U(IV) (②). The formation of the final oxide precipitate occurs through the hydrolysis of the U^{4+} cations and proceeds first *via* the formation of colloids in solution, probably in the hydroxylated form (③), which then aggregate to give rise to the first solid nuclei. The latter then grow to form micrometric single crystals of UO_{2+x} (④).

5. Conclusion

The study of the hydrothermal conversion of a solution containing uranium(VI) and oxalate ions, as a simplified model of the uranium(VI)–metal(IV) system, has demonstrated that it was possible to convert molecular uranyl cations into uranium(IV) oxide and to specify the experimental conditions influencing the physicochemical properties of the samples obtained. Particularly, pH has a considerable effect on uranium reduction, the precipitation yield and the nature of the precipitated uraniferous phases varying drastically over a very narrow pH range. Optimal parameters for quantitative hydrothermal conversion of the reaction mixture into UO_{2+x} were thus identified, with a conversion time of over 72 hours and an initial pH set at 0.8 at T = 250 °C. Using these conditions, uranium(VI) was thus quantitatively reduced to uranium(IV) without any addition of a reducing agent other than oxalates.

To gain a better understanding of the redox mechanisms involved in the hydrothermal conversion of uranium(VI) to UO_{2+x} by oxalates, *in situ* XANES analyses were carried out. The study focused on monitoring the uranium oxidation state in solution and within the precipitate formed rapidly during hydrothermal treatment. The study of the solution revealed an almost complete reduction of uranium(VI) into uranium(IV), as well as a change in the uranium complexation, probably caused by the decomposition of oxalate ions under the effect of the pressure–temperature couple. Similarly, the drop in uranium fluorescence intensity in solution was explained by rapid U(IV) precipitation. Furthermore, uranium(IV) appears to precipitate directly as UO_{2+x}, and no variation in the oxidation state of uranium within the solid could be demonstrated under the conditions of the experiments.

This study thus demonstrates that the hydrothermal conversion of actinide oxalates into oxides is an extremely versatile tool that can be implemented in a large variety of chemical systems, including a large range of oxidation states for the cations initially present in solution. This could lead to a wider range of potential applications for such methods within the nuclear fuel cycle, especially if solid solutions can be obtained. The next step will then be to use hydrothermal reductive conversion within a more complex system, with the aim to obtain mixed oxides based on uranium(IV) and the tetravalent metal cation M(IV).

Author contributions

S. Benarib: investigation, data curation, and writing – original draft; M. Munoz: investigation; I. Kieffer: investigation and writing – review & editing; J.-L. Hazemann: investigation and writing – review & editing; N. Dacheux: supervision and writing – review & editing; N. Clavier: project administration, supervision, and writing – original draft.

Data availability

The data supporting the findings of this study are available within the paper and as part of the Supplementary Information. Should any raw data files be needed in another

format, they are available from the corresponding author upon request.

Conflicts of interest

There are no conflicts to declare.

Acknowledgements

The authors thank ESRF for providing beamtime and access to the synchrotron facilities. They would like to particularly acknowledge P. Collomp for his help in setting up the experiments involving radioactive samples on the FAME beamline. The HP/HT vessel was financially supported by the French "Grand Emprunt" EquipEx (PlanEx, ANR-11-EQPX-36). The authors would also like to thank CEA for funding the PhD work of Sofian Benarib. This research contributes to the SESAM pilot-project of the Joint Program on Nuclear Materials (JPNM) of the European Energy Research Alliance (EERA).

References

1 T. Abe and K. Asakura, Uranium oxide and MOX production, in *Comprehensive nuclear materials*, ed. R. J. M. Konings, T. R. Allen, R. E. Stoller and S. Yamanaka, Elsevier, Amsterdam, 2012, pp. 393–422.
2 Z. Talip, S. Peuget, M. Magnin, M. Tribet, C. Valot, R. Vauchy and C. Jegou, Characterization of un-irradiated MIMAS MOX fuel by Raman spectroscopy and EPMA, *J. Nucl. Mater.*, 2018, **499**, 88–97.
3 G. Oudinet, I. Munoz-Viallard, L. Aufore, M. J. Gotta, J. M. Becker, G. Chlarelli and R. Castelli, Characterization of plutonium distribution in MIMAS MOX by image analysis, *J. Nucl. Mater.*, 2008, **375**, 86–94.
4 F. Abraham, B. Arab-Chapelet, M. Rivenet, C. Tamain and S. Grandjean, Actinide oxalates, solid state structures and applications, *Coord. Chem. Rev.*, 2014, **266–267**, 28–68.
5 J. Martinez, N. Clavier, A. Mesbah, F. Audubert, X. F. Le Goff, N. Vigier and N. Dacheux, An original precipitation route toward the preparation and the sintering of highly reactive uranium cerium dioxide powders, *J. Nucl. Mater.*, 2015, **462**, 173–181.
6 A. Hautecouverture, P. Estevenon, C. Rey and X. Deschanels, Synthesis of plutonium dioxide by citric acid-assisted solution combustion synthesis, *J. Nucl. Mater.*, 2023, **586**, 154694.
7 C. Chambon, S. Vaudez and J. M. Heintz, De-densification mechanisms of yttria-doped cerium oxide during sintering in a reducing atmosphere, *J. Am. Ceram. Soc.*, 2018, **101**, 4956–4967.
8 O. Walter, K. Popa and O. Dieste Blanco, Hydrothermal decomposition of actinide(IV) oxalates: a new aqueous route towards reactive actinide oxide nanocrystals, *Open Chem.*, 2016, **14**, 170–174.
9 K. Popa, O. Walter, O. D. Blanco, A. Guiot, D. Bouexiere, J. Y. Colle, L. Martel, M. Naji and D. Manara, A low-temperature synthesis method for AnO_2 nanocrystals (An = Th, U, Np, and Pu) and associate solid solutions, *CrystEngComm*, 2018, **20**, 4614–4622.
10 J. Manaud, J. Maynadie, A. Mesbah, M. O. J. Y. Hunault, P. Martin, M. Zunino, N. Dacheux and N. Clavier, Hydrothermal Conversion of Thorium Oxalate into into $ThO_2{\cdot}nH_2O$ oxide, *Inorg. Chem.*, 2020, **59**, 14954–14966.
11 J. Manaud, J. Maynadie, A. Mesbah, M. O. J. Y. Hunault, P. M. Martin, M. Zunino, D. Meyer, N. Dacheux and N. Clavier, Hydrothermal Conversion of Uranium(IV) Oxalate into Oxides: A Comprehensive Study, *Inorg. Chem.*, 2020, **59**, 3260–3273.
12 S. Benarib, N. Dacheux, X. F. Le Goff, J. Lautru, L. D. Mascio and N. Clavier, Hydrothermal conversion of mixed uranium(IV)-cerium(III) oxalates into $(U,Ce)O_2{\cdot}nH_2O$ solid solutions, *Dalton Trans.*, 2023, **52**, 10951–10968.
13 W. Liu, L. J. Feng, C. Zhang, H. X. Yang, J. X. Guo, X. F. Liu, X. Y. Zhang and Y. Z. Yang, A facile hydrothermal synthesis of 3D flowerlike CeO_2 via a cerium oxalate precursor, *J. Mater. Chem. A*, 2013, **1**, 6942–6948.
14 S. Nakashima, J. R. Disnar, A. Perruchot and J. Trichet, Fixation and Reduction of Uranium by Natural Organic-Matter - Reaction-Mechanisms and Kinetics, *Bull. Mineral.*, 1987, **110**, 227–234.
15 S. Nakashima, J. R. Disnar, A. Perruchot and J. Trichet, Experimental-Study of Mechanisms of Fixation and Reduction of Uranium by Sedimentary Organic-Matter under Diagenetic or Hydrothermal Conditions, *Geochim. Cosmochim. Acta*, 1984, **48**, 2321–2329.
16 S. Nakashima, Complexation and Reduction of Uranium by Lignite, *Sci. Total Environ.*, 1992, **118**, 425–437.
17 S. Nakashima, Kinetics and Thermodynamics of U-Reduction by Natural and Simple Organic-Matter, *Org. Geochem.*, 1992, **19**, 421–430.
18 C. Tabata, K. Shirasaki, A. Sunaga, H. Sakai, D. X. Li, M. Konaka and T. Yamamura, Supercritical hydrothermal synthesis of UO_{2+x}: stoichiometry, crystal shape and size, and homogeneity observed using ^{23}Na-NMR spectroscopy of $(U, Na)O_{2+x}$, *CrystEngComm*, 2021, **23**, 8660–8672.
19 K. Shirasaki, C. Tabata, A. Sunaga, H. Sakai, D. X. Li, M. Konaka and T. Yamamura, Homogeneity of $(U, M)O_2$ (M = Th, Np) prepared by supercritical hydrothermal synthesis, *J. Nucl. Mater.*, 2022, **563**, 153608.
20 D. Hudry, J. C. Griveau, C. Apostolidis, O. Walter, E. Colineau, G. Rasmussen, D. Wang, V. S. K. Chakravadhaluna, E. Courtois, C. Kübel and D. Meyer, Thorium/uranium mixed oxide nanocrystals: Synthesis, structural characterization and magnetic properties, *Nano Res.*, 2014, **7**, 119–131.
21 D. Hudry, C. Apostolidis, O. Walter, T. Gouder, A. Janssen, E. Courtois, C. Kübel and D. Meyer, Synthesis of transuranium-based nanocrystals via the thermal decomposition of actinyl nitrates, *RSC Adv.*, 2013, **3**, 18271–18274.

22 D. Ferri, M. Iuliano, C. Manfredi, E. Vasca, T. Caruso, M. Clemente and C. Fontanella, Dioxouranium(VI) oxalate complexes, *J. Chem. Soc., Dalton Trans.*, 2000, 3460–3466.
23 N. C. Jayadevan and D. M. Chackraburtty, Crystal and Molecular-Structure of Uranyl Oxalate Trihydrate, *Acta Crystallogr., Sect. B: Struct. Sci., Cryst. Eng. Mater.*, 1972, **28**, 3178–3182.
24 B. H. Toby and R. B. Von Dreele, GSAS-II: the genesis of a modern open-source all purpose crystallography software package, *J. Appl. Crystallogr.*, 2013, **46**, 544–549.
25 L. Desgranges, G. Baldinozzi, G. Rousseau, J. C. Niepce and G. Calvarin, Neutron Diffraction Study of the in Situ Oxidation of UO_2, *Inorg. Chem.*, 2009, **48**, 7585–7592.
26 O. Proux, X. Biquard, E. Lahera, J. J. Menthonnex, A. Prat, O. Ulrich, Y. Soldo, P. Trévisson, G. Kapoujyan, G. Perroux, P. Taunier, D. Grand, P. Jeantet, M. Deleglise, J. P. Roux and J. L. Hazemann, FAME : A new beamline for X-ray absorption investigations of very-diluted systems of environmental, material and biological interests, *Phys. Scr.*, 2005, **T115**, 970–973.
27 D. Testemale, R. Argoud, O. Geaymond and J. L. Hazemann, High pressure high temperature cell for X-ray absorption and scattering techniques, *Rev. Sci. Instrum.*, 2005, **76**, 043905.
28 D. Testemale, A. Prat, E. Lahera and J. L. Hazemann, Novel high-pressure windows made of glass-like carbon for X-ray analysis, *Rev. Sci. Instrum.*, 2016, **87**, 075115.
29 R. J. Finch, F. C. Hawthorne and R. C. Ewing, Structural relations among schoepite, metaschoepite and "dehydrated schoepite", *Can. Mineral.*, 1998, **36**, 831–845.
30 L. Desgranges, G. Badinozzi, D. Simeone and H. E. Fischer, Refinement of the a-U_4O_9 Crystalline Structure: New Insight into the $U_4O_9 \rightarrow U_3O_8$ Transformation, *Inorg. Chem.*, 2011, **50**, 6146–6151.
31 G. Leinders, T. Cardinaels, K. Binnemans and M. Verwerft, Accurate lattice parameter measurements of stoichiometric uranium dioxide, *J. Nucl. Mater.*, 2015, **459**, 135–142.
32 K. Sangwal, C. C. Desai and V. John, Etch Pit Morphology and Calcium-Sulfate Growth on [111] Faces of Calcium-Fluoride Crystals Etched in Sulfuric-Acid, *Krist. Tech.*, 1979, **14**, 63–72.
33 S. Bertolotto, S. Szenknect, S. Lalleman, A. Magnaldo, P. Raison, M. Odorico, R. Podor, L. Claparede and N. Dacheux, Effect of surface orientation on dissolution rate and surface dynamics of UO_2 single crystals in nitric acid, *Corros. Sci.*, 2020, **176**, 109020.
34 O. Riba, C. Walker and K. V. Ragnarsdottir, Kinetic studies of synthetic metaschoepite under acidic conditions in batch and flow experiments, *Environ. Sci. Technol.*, 2005, **39**, 7915–7920.
35 H. Ding, M. C. D. Wilkins, C. Gausse, L. M. Mottram, S. K. Sun, M. C. Stennett, D. Grolimund, R. Tappero, S. Nicholas, N. C. Hyatt and C. L. Corkhill, Safely probing the chemistry of Chernobyl nuclear fuel using micro-focus X-ray analysis, *J. Mater. Chem. A*, 2021, **9**, 12612–12622.
36 S. Finkeldei, M. C. Stennett, P. M. Kowalski, Y. Ji, E. de Visser-Tynová, N. C. Hyatt, D. Bosbach and F. Brandt, Insights into the fabrication and structure of plutonium pyrochlores, *J. Mater. Chem. A*, 2020, **8**, 2387–2403.
37 E. L. Shock, D. C. Sassani and H. Betz, Uranium in geologic fluids: Estimates of standard partial molal properties, oxidation potentials, and hydrolysis constants at high temperatures and pressures, *Geochim. Cosmochim. Acta*, 1997, **61**, 4245–4266.
38 L. Duvieubourg-Garela, N. Vigier, F. Abraham and S. Grandjean, Adaptable coordination of U(IV) in the 2D-(4,4) uranium oxalate network: From 8 to 10 coordinations in the uranium(IV) oxalate hydrates, *J. Solid State Chem.*, 2008, **181**, 1899–1908.
39 H. Moll, M. A. Denecke, F. Jalilehvand, M. Sandström and I. Grenthe, Structure of the aqua ions and fluoride complexes of uranium(IV) and thorium(IV) in aqueous solution an EXAFS study, *Inorg. Chem.*, 1999, **38**, 1795–1799.
40 H. Moll, T. Reich and Z. Szabó, The hydrolysis of dioxouranium(VI) investigated using EXAFS and ^{17}O-NMR, *Radiochim. Acta*, 2000, **88**, 411–415.
41 B. Ravel and M. Newville, ATHENA, ARTEMIS, HEPHAESTUS: data analysis for X-ray absorption spectroscopy using IFEFFIT, *J. Synchrotron Radiat.*, 2005, **12**, 537–541.
42 R. Bès, T. Ahopelto, A. P. Honkanen, S. Huotari, G. Leinders, J. Pakarinen and K. Kvashnina, Laboratory-scale X-ray absorption spectroscopy approach for actinide research: Experiment at the uranium L_3-edge, *J. Nucl. Mater.*, 2018, **507**, 50–53.
43 G. Leinders, R. Bes, J. Pakarinen, K. Kvashnina and M. Verwerft, Evolution of the Uranium Chemical State in Mixed-Valence Oxides, *Inorg. Chem.*, 2017, **56**, 6784–6787.
44 E. A. Hudson, J. J. Rehr and J. J. Bucher, Multiple-Scattering Calculations of the Uranium L(3)-Edge X-Ray-Absorption near-Edge Structure, *Phys. Rev. B: Condens. Matter Mater. Phys.*, 1995, **52**, 13815–13826.
45 S. D. Conradson, B. D. Begg, D. L. Clark, C. den Auwer, M. Ding, P. K. Dorhout, F. J. Espinosa-Faller, P. L. Gordon, R. G. Haire, N. J. Hess, R. F. Hess, D. W. Keogh, G. H. Lander, D. Manara, L. A. Morales, M. P. Neu, P. Paviet-Hartmann, J. Rebizant, V. V. Rondinella, W. Runde, C. D. Tait, D. K. Veirs, P. M. Villella and F. Wastin, Charge distribution and local structure and speciation in the UO_{2+x} and PuO_{2+x} binary oxides for $x \leq 0.25$, *J. Solid State Chem.*, 2005, **178**, 521–535.
46 D. Prieur, M. M. Desagulier, D. R. Neuville, C. Guéneau, E. Epifano, K. Dardenne, J. Rothe and P. Martin, A spectroscopic hike in the U-O phase diagram, *J. Synchrotron Radiat.*, 2021, **28**, 1684–1691.
47 J. M. Elorrieta, L. J. Bonales, N. Rodriguez-Villagra, V. G. Baonza and J. Cobos, A detailed Raman and X-Ray study of UO_{2+x} oxides and related structure transitions, *Phys. Chem. Chem. Phys.*, 2016, **18**, 28209–28216.
48 R. Vauchy, S. Hirooka and T. Murakami, Ionic radii in fluorites, *Materialia*, 2023, **32**, 101934.

49 M. H. Weik, Electrochemical series, in: *Computer Science and Communications Dictionary*, Springer US, Boston, MA, 2001, pp. 489–489.
50 J. Schneider, H. F. Jia, J. T. Muckerman and E. Fujita, Thermodynamics and kinetics of CO_2, CO, and H^+ binding to the metal centre of CO_2 reduction catalysts, *Chem. Soc. Rev.*, 2012, **41**, 2036–2051.
51 A. O. Pavlyuk, E. V. Bespala, S. G. Kotlyarevskii, V. S. Zagumennov, E. V. Zakharova, A. G. Volkova and N. I. Rodygina, Electrochemical Decontamination of Irradiated Nuclear Graphite of Uranium-Graphite Nuclear Reactors, *At. Energy*, 2020, **128**, 24–29.
52 S. R. Qiang, J. J. Wang, Y. Wang, L. M. Yuan, L. P. Shi, Z. Ding, W. Wang, J. J. Liang, P. Li and Q. H. Fan, Analysis of the uranium chemical state by XPS: Is what you see real?, *Appl. Surf. Sci.*, 2022, **576**, 151886.
53 E. S. Ilton, J. F. Boily and P. S. Bagus, Beam induced reduction of U(VI) during X-ray photoelectron spectroscopy: The utility of the U 4f satellite structure for identifying uranium oxidation states in mixed valence uranium oxides, *Surf. Sci.*, 2007, **601**, 908–916.
54 V. Neck and J. I. Kim, Solubility and hydrolysis of tetravalent actinides, *Radiochim. Acta*, 2001, **89**, 1–16.
55 D. F. Johnson, K. Bhaskaran-Nair, E. J. Bylaska and W. A. de Jong, Thermodynamics of Tetravalent Thorium and Uranium Complexes from First-Principles Calculations, *J. Phys. Chem. A*, 2013, **117**, 4988–4995.
56 C. Micheau, M. Virot, S. Dourdain, T. Dumas, D. Menut, P. L. Solari, L. Venault, O. Diat, P. Moisy and S. I. Nikitenko, Relevance of formation conditions to the size, morphology and local structure of intrinsic plutonium colloids, *Environ. Sci.: Nano*, 2020, **7**, 2252–2266.